Editors' Suggestion

Nonmonotonic Hall Effect of Weyl Semimetals under a Magnetic Field

Xiao-Xiao Zhang[1,*] and Naoto Nagaosa[2,3,†]
[1]Wuhan National High Magnetic Field Center and School of Physics, Huazhong University of Science and Technology, Wuhan 430074, China
[2]RIKEN Center for Emergent Matter Science (CEMS), Wako, Saitama 351-0198, Japan
[3]Fundamental Quantum Science Program, TRIP Headquarters, RIKEN, Wako, Saitama 351-0198, Japan

(Received 29 April 2024; revised 25 July 2024; accepted 15 August 2024; published 16 October 2024)

The Hall effect of topological quantum materials often reveals essential new physics and possesses potential for application. The magnetic Weyl semimetal is one especially interesting example that hosts an interplay between the spontaneous time-reversal symmetry-breaking topology and the external magnetic field. However, it is less known beyond the anomalous Hall effect thereof, which is unable to account for plenty of magnetotransport measurements. We propose a new Hall effect characteristically nonmonotonic with respect to the external field, intrinsic to the three-dimensional Weyl topology, and free from chemical potential fine-tuning. Two related mechanisms from the Landau level bending and chiral Landau level shifting are found, together with their relation to the Shubnikov–de Hass effect. This field-dependent Hall response, universal to thin films and bulk samples, provides a concrete physical picture for existing measurements and is promising to guide future experiments.

DOI: 10.1103/PhysRevLett.133.166301

Introduction—The Hall effect and related magnetotransport have long been a constant source of new physics for solid-state systems. The recent surge of topological quantum materials significantly invigorated the relevant transport study. The Weyl semimetal (WSM) is a three-dimensional (3D) epitome and surpasses the two-dimensional (2D) Dirac physics [1–10]. Its linear band crossings as Weyl points (WPs) and unique topology bring about many interesting phenomena. Without an applied magnetic field, the surface circulating states due to slices between WPs can produce an anomalous Hall effect (AHE) as a hallmark of magnetic WSMs [11,12]. Such time-reversal $\mathcal{T}$-breaking systems were predicted theoretically [13–21] with an appealing interplay between magnetism and topology, and experimentally investigated in Mn_3Sn [22,23], GdPtBi [24–27], $Co_3Sn_2S_2$ [28–32], etc.

The magnetotransport thereof in the Hall channel is usually crudely decomposed as the magnetic field B-linear ordinary Hall effect (OHE) and the magnetization-induced AHE. This, however, often fails to account for the rich field-dependent Hall effects observed. They are typically nonlinear and nonmonotonic in B and not due to hysteresis, whose mechanism remains unclear [25,26,28,33–35]. Theoretically, this oversimplified picture also contradicts the intuition that the WSM topology should enter more nontrivially into the Hall effect at finite fields. This becomes especially true when the quantum effects of magnetic fields are properly taken into account with Landau level (LL) formation. WSMs with relativistic band structure and intriguing 3D topology should naturally accommodate special LLs, associated with nontrivial field dependence and influence on the Hall response [7,8]. Here, we address this issue and propose a nonmonotonic field-dependent Hall effect in a magnetic WSM, combining the intrinsic $\mathcal{T}$-breaking topology and the field-induced quantum effects of LLs. Given the universal mechanism, this Hall effect is present in both thin films and bulk samples; neither does it require fine-tuning the chemical potential close to WPs while many other transport features of WSM demand. It therefore represents a new Hall effect at the crossroads between topology, spontaneous $\mathcal{T}$ breaking, and external magnetic field. By revealing this Hall effect in comparison to experimental results, a promising physical picture for the foregoing measurements is provided.

Model system and Hall response—We start from a minimal $\mathcal{T}$-breaking WSM lattice Hamiltonian $H(\boldsymbol{k}) = t_1(\chi \sin k_x\sigma_x + \sin k_y\sigma_y) + [t_0(\cos k_z - \cos \bar{k}_z) + t\sum_{i=x,y}(\cos k_i - \cos \bar{k}_i)]\sigma_z$ with chirality $\chi = \pm$, Pauli matrix σ, and a pair of zero-energy WPs at $\pm\bar{\boldsymbol{k}} = (0, 0, \pm k_w)$ illustrated in Fig. 1(a). For concreteness, we assume $t_0, t_1, t > 0$ and leave other cases to the Supplemental Material (SM) [36]. The corresponding continuum model we mainly rely on reads

$$h(\boldsymbol{k}) = t_1(\chi k_x\sigma_x + k_y\sigma_y) + [m(k_z) - t(k_x^2 + k_y^2)/2]\sigma_z \qquad (1)$$

with $m(k_z) = m_0 - (t_0/2)k_z^2$ and $m_0 = t_0(1 - \cos k_w)$. Equation (1) differs from usual Dirac models by including t, the natural high-energy regularization from the lattice.

*Contact author: xxzhang@hust.edu.cn
†Contact author: nagaosa@riken.jp

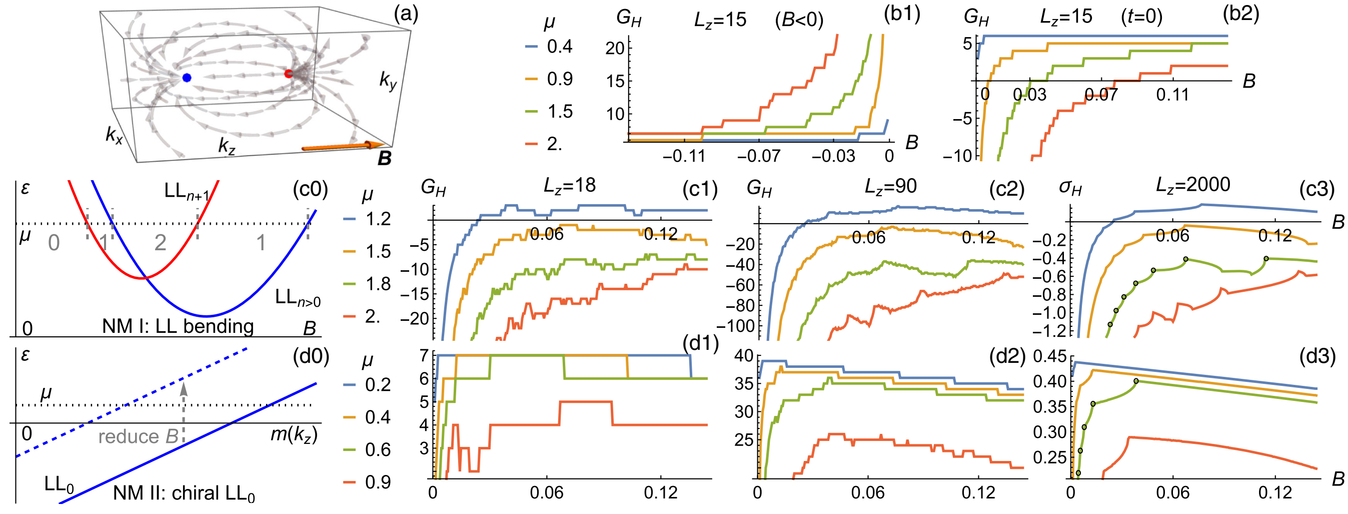

FIG. 1. (a) Schematic model system: a pair of positive (red) and negative (blue) WPs are aligned along the k_z axis; gray Berry curvature streamlines connect WPs and represent the intrinsic $\mathcal{T}$-breaking topology, which is at interplay with the orange external magnetic field $\boldsymbol{B}\|\hat{z}$. (b) Purely monotonic Hall signals when (b1) $B<0$ or (b2) $t=0$ in contrast to their nonmonotonic counterpart (c1), (d1). (c0), (d0) Both nonmonotonic mechanisms (NM I and II) of the Hall effect originate from intrinsic WSM topology. (c0) Represented by two bent and reshuffled LL_n and LL_{n+1}, NM I exploits the anomalously nonmonotonic occupation change (numbers below dotted chemical potential μ) when B is reduced; (d0) NM II relies on the field-induced shift of chiral LL_0 and the associated occupation change in relevant $m(k_z)$ slices. [(c1)–(c3), (d1)–(d3)] Nonmonotonic Hall signals dependent on chemical potential μ and thickness L_z: (c1), (c2), (d1), (d2) thin films or mesoscopic samples (conductance G_H in units of e^2/h); (c3), (d3) bulk samples (3D conductivity $\sigma_H=G_H/L_z$). Parameters are $\chi=-1$, $t_1=3$, $t_0=4$, $t=12$, $k_w=\pi/2$. (c1)–(c3) Higher μ clearly shows NM I often with irregular nonmonotonicity while NM II also participates. (d1)–(d3) As μ decreases across the minimal threshold energy $\mathcal{M}_1=0.75$ for NM I, generally more irregular signals transition to regular NM II signals with one major nonmonotonic turn. (c3), (d3) clearly show the Shubnikov-de Haas effect (SdHE) with successive cusps, circled representatively in green curves, modified by nonmonotonicity to acquire unconventional periodicity.

Only by this, the essential lattice WSM topology is properly captured, otherwise it would suffer from parity anomaly and half-quantized Chern number for any 2D k_z-section [37,38]. With t, Chern numbers are integer quantized: topologically nontrivial (trivial) between (outside) the WPs. This complete global topology of realistic WSMs will significantly impact Hall effects, later proved to be an indispensable ingredient of any nonmonotonic behavior. Applying a magnetic field $B\hat{z}$ for a sample of thickness L_z along the z axis, the allowed discrete k_z's are conserved and Eq. (1) becomes an effective 2D model of each $m(k_z)$ slice. The general $\mathrm{LL}_{n\neq 0}$ reads $\varepsilon_n=\bar{\varepsilon}+\mathrm{sgn}(n)\sqrt{(m-2|n|u_B)^2+|n|v_B^2}$ with $m=m(k_z)$ while the special LL_0 $\varepsilon_0=\bar{\varepsilon}-\chi bm$ is chiral in the (m,ε) plane, where $\bar{\varepsilon}=\chi bu_B, u_B=t/2l_B^2, v_B=\sqrt{2t_1^2/l_B^2}$ and magnetic length $l_B=\sqrt{\hbar/e|B|}$ with $b=\mathrm{sgn}(B)$ the sign of the field.

Detailed in SM I, the Hall conductance of Eq. (1) for a particular k_z can be separated as $G_H=\bar{G}_H+\Delta G_H$. Measured in units of e^2/h,

$$\bar{G}_H=-\chi[\mathrm{sgn}(m)+\mathrm{sgn}(t)]/2, \tag{2}$$

independent of the chemical potential μ and B, and due to the intrinsic topology, is apparently the same as the zero-field Hall effect from topological insulator thin films and contributes to the foregoing AHE in WSMs [39].

$$\Delta G_H=-b\nu\Theta(\Delta)\Theta(n_L-n_R)(n_L-n_R+1) \tag{3}$$

reflects the topology influenced by magnetic field and occupation, where $n_L=\max[-1,\lfloor n_+\rfloor], n_R=\max[\xi,\lceil n_-\rceil]$ and $n_\pm=[(4mu_B-v_B^2\pm\sqrt{\Delta})/(8u_B^2)]$ with $\Delta=v_B^2(v_B^2-8mu_B)+16u_B^2(\mu-\bar{\varepsilon})^2$, $\xi=[1+\mathrm{sgn}(m)\chi b\nu]/2$, and $\nu=\mathrm{sgn}(\mu-\bar{\varepsilon})$ switching sign between electronlike and holelike contributions. $\Theta(x)$ is the step function and $\lfloor x\rfloor$ ($\lceil x\rceil$) denotes the greatest (smallest) integer less (greater) than or equal to x. $n_{L,R}$ signifies the proper LL index regarding the left/right crossing of chemical potential. The physical motivation is to count LLs filled with respect to the gapped region near the band midpoint; Θ functions guarantee such fillings and associated quantized contributions from LLs are picked up. With these analytic formulae, one can sum over the $m(k_z)$ slices and find the full conductance $G_H=\sum_{k_z}G_H[m(k_z)]$ dependent on L_z measured in the lattice constant, as shown in Fig. 1. G_H satisfies

$$G_H(B,\mu)=G_H(-B,-\mu) \tag{4}$$

related to the particle-hole symmetry breaking and the Onsager reciprocal relations (SM II). The B asymmetry

$G_H(B,\mu) \neq G_H(-B,\mu)$ implied in Eq. (4) originates from the $\mathcal{T}$ breaking in our magnetic WSM and will manifest drastically in the nonmonotonic Hall effect.

In the conventional 2D electron gas or graphene [40], the number of filled/empty LLs always increases with decreasing $|B|$ as they are pushed toward the band midpoint with monotonically decreasing LL spacings. This leads to a common monotonic $G_H(B)$ as in the quantum Hall effect. When $b\mu < 0$ or $t = 0$, Figs. 1(b1) and 1(b2) follow the same conventional behavior (see also SM Fig. S1). Remarkably, when $b\mu > 0$, Figs. 1(c) and 1(d) stably exhibit a nonmonotonic $G_H(B)$ in a wide field window, except the downturn at small B also due to the conventional LL spacing effect. Note, however, that such an apparent divergence with $B \to 0$ will only be regularized to the OHE as $G_H \propto \omega_c \tau \propto B$ with cyclotron frequency ω_c and relaxation time τ due to realistic scatterings (SM III).

Nonmonotonic mechanism I: LL bending and reshuffling—To understand the nonmonotonic behavior, one notices a unique $\mathrm{LL}_{n\neq 0}$ bending phenomenon of the WSM exemplified in Fig. 1(c0), i.e., sign switching of the LL slope or nonmonotonic movement of the LL with $|B|$. Once any filled LL bends upward with decreasing $|B|$, it is possible to be emptied when the fixed μ crosses it again at a lower $|B|$, resulting in the opposite Hall contribution. With this nonmonotonic mechanism (denoted as NM I), there are multiple nonmonotonic turns, dependent intricately on B, μ, the variable momentum slice $m(k_z)$, and the participating LLs. Hence the robust but often irregular nonmonotonic behavior in Figs. 1(c1)–1(c3). We find a sufficient condition for NM I (SM IV A)

$$m(k_z) > -\chi b\mu > \mathcal{M}_n \tag{5}$$

with a threshold energy $\mathcal{M}_n = |n| t_1^2/t$ linked to LL index n. Since $\mathcal{M}_n$ increases with $|n|$, any $\mathrm{LL}_{|l|\leq|n|}$ can participate NM I, as summarized in Table I. Intuitively, to pick up the nonmonotonic occupation change in Fig. 1(c0), μ must cross LLs; the constraint on $|\mu|$ from $\mathcal{M}_n$ to $m(k_z)$ follows from the relevant LL extrema. Bending LLs are often accompanied by the reshuffling of LL ordering, e.g., anomalous $\varepsilon_{n+1} < \varepsilon_n$ exemplified in Fig. 1(c0). This complementary view can retain explicit $|B|$ dependence and is explored in SM IV B.

Crucially, it is the quadratic t term in Eq. (1) that enables LL bending or reshuffling in Fig. 1(c0). Without it, LLs do not bend, divergent $\mathcal{M}_n$ renders the condition Eq. (5) never fulfilled, and transport returns to the conventional purely monotonic behavior shown in Fig. 1(b2). As aforementioned, finite t is essential to capture the nontrivial and realistic global WSM topology. Therefore, NM I is a direct and intrinsic signature of the WSM topology under magnetic field.

Equation (5) immediately suggests more bending LLs accommodated and hence typically stronger nonmonotonicity with higher $|\mu|$, corroborated by Figs. 1(c1)–1(c3)

TABLE I. Relations among two nonmonotonic mechanisms and SdHE. They summarize Eqs. (5), (6), and (7). Leftmost conditions are specified with a threshold energy $\mathcal{M}_n$ linked to LL index n and dependent on chemical potential μ, WSM chirality χ, and the sign of magnetic field b. Fixing such conditions, the presence (✓) or absence (-) of the corresponding phenomena due to generic LL_l can be given in relation to fixed n. NM I and SdHE due to the same LL (distinct LLs) cannot (can) coexist. NM II persists regardless of $\mathcal{M}_n$. Nonmonotonic Hall effect disappears when $-\chi b\mu \leq 0$.

	NM I (LL bending)	NM II (chiral LL_0)	SdHE
$-\chi b\mu \leq 0$	-	-	all LL: ✓
$0 < -\chi b\mu < \mathcal{M}_n$	$\mathrm{LL}_{\lvert l\rvert\geq\lvert n\rvert}$: -	✓	$\mathrm{LL}_{\lvert l\rvert\geq\lvert n\rvert}$: ✓
$-\chi b\mu > \mathcal{M}_n$	$\mathrm{LL}_{\lvert l\rvert\leq\lvert n\rvert}$: ✓	✓	$\mathrm{LL}_{\lvert l\rvert\leq\lvert n\rvert}$: -

and also its comparison with Figs. 1(d1)–(d3). Besides, reducing μ eventually across the threshold minimum $\mathcal{M}_1$, Figs. 1(d1)–1(d3) shows a pattern shift to a distinctly more regular nonmonotonicity (discussed later). Equation (5) also manifests the aforementioned B asymmetry in a remarkable way. Exemplifying with $\chi = -1$, only $b > 0$, $\mu > 0$ and $b < 0$, $\mu < 0$ related by Eq. (4) can show the nonmonotonicity while other cases rarely do (SM IV C). This thus becomes a drastic feature of the $\mathcal{T}$ breaking in the WSM system.

Shubnikov–de Haas effect—During the reduction of $|B|$, the Hall signal especially for a bulk sample will also exhibit a Shubnikov–de Haas effect (SdHE). Such contribution from LL spacing reduction is itself monotonic as aforementioned and thus causes cusps rather than direct oscillations as shown in Figs. 1(c3) and 1(d3). A cusp at $|B|_n$ appears once μ touches the extremum of a particular $\mathrm{LL}_{n\neq 0}$ in any $m(k_z)$ slice, provided that (SM V A)

$$-\chi b\mu < \mathcal{M}_n. \tag{6}$$

The foregoing finite t crucial to the WSM makes the cusp separation $\Delta|B|_n^{-1}$ nonuniform, in contrast to the conventional case.

Intriguingly, Eq. (6) and Eq. (5) from two distinct viewpoints are mutually exclusive. Their connection can be rigorously built by considering the LL energy surface in the 3D $(m, |B|, \varepsilon)$ space and its extremal curves (SM V B). Intuitively speaking, the LL bending effect requires μ crossing a LL and hence it hardly reaches the extremum to induce any SdHE kinks. This important relation enriches Table I for two nonmonotonic mechanisms and SdHE. It is, however, worth pointing out that the two *phenomena*, SdHE and nonmonotonicity due to LL bending, are not exclusive. SdHE cusps due to $\mathrm{LL}_{|l|\geq|n|}$ can occur while $\mathrm{LL}_{|l|<|n|}$ bending may still coexist if parameters allow $-\chi b\mu > \mathcal{M}_{|l|<|n|}$, e.g., one can observe SdHE following nonmonotonicity as $|B|$ decreases, seen in Fig. 1(c3). This clarifies the no-go (2, 1)-entry and the similar (3, 3)-entry in Table I.

Nonmonotonic mechanism II: Chiral LL_0—As aforementioned and clearly suggested by Figs. 1(d1)–1(d3), there exists another indispensable nonmonotonic mechanism (NM II). It gives rise to a distinctly more regular nonmonotonic variation in $G_H(B)$ than NM I: the profile typically exhibits one overall nonmonotonic turn before approaching the $|B| \sim 0$ region, although it possibly consists of multiple steps for a thin film as in Figs. 1(d1) and 1(d2). Illustrated in Fig. 1(d0), this originates from the unique chiral LL_0 movement that shifts linearly with $|B|$ as per $\partial\varepsilon_0/\partial|B| = et\chi b/2\hbar$. Given μ, this changes the occupation in momentum slices and hence G_H in a nontrivial way (SM III): the change is opposite to the foregoing conventional effect of LL spacing reduction if and only if

$$-\chi b\mu > 0. \tag{7}$$

These two opposite contributions to $G_H(B)$ naturally lead to nonmonotonicity and its condition above complies with Eq. (4). NM II will also modify and compete with SdHE, because SdHE follows the monotonic behavior.

Equation (7) is also a necessary condition of Eq. (5) for LL bending. Hence, NM I and II are inclusive of each other under Eq. (7) and will contribute constructively together when the system parameters permit as in Figs. 1(c1)–1(c3). NM II is not limited by the mass range $m_0 > \mathcal{M}_1$ implicitly implied by Eq. (5) and can always contribute. Especially, if $|\mu|$ or t is too small to fulfill Eq. (5), typically when $|\mu|$ is close to or below the threshold minimum $\mathcal{M}_1$, NM II becomes the major cause of nonmonotonicity, as aforementioned and shown in Figs. 1(d1)–1(d3).

It is important to realize that NM II is also a direct consequence of the same finite t as NM I. It now generates the field-dependent shift of LL_0 in Fig. 1(d0) and is crucial to nonmonotonicity as suggested by Fig. 1(b2), where neither of two NMs exists. Again, the nonmonotonicity traces intrinsically back to the generic 3D global WSM topology. In fact, although both NMs considerably rely on 2D Dirac physics, the WSM provides the natural embedding in 3D with the requisite regularization and a whole family of different 2D slices. This crucially removes any necessity of fine-tuning and solidifies nonmonotonicity, in a way reminiscent of the generic appearance of WPs in 3D.

Thick sample situation—For a bulk sample of large L_z, the allowed quantized k_z's form a continuum and we have instead the bulk 3D conductivity $\sigma_H = G_H/L_z = (1/\pi)\int \mathrm{d}k_z G_H[m(k_z)]$. As clearly shown in Figs. 1(c3) and 1(d3), NM I and II are not limited to a thin sample of a few atomic layers or mesoscopic scale. Traversing the relevant LLs, the integral will stably pick up both the conventional monotonic part and the two nonmonotonic contributions. However, the conductance variation in discrete steps, which strongly depend on the system details and thickness, will be considerably smoothed out. Therefore, not only do NM I and II survive, but the Hall signal can become simpler with fewer irregular nonmonotonic changes.

There are also differences between NM I and II. NM II is scale invariant due to the chiral feature of LL_0, making NM II almost intact from parameter changes. Only the signal becomes less discrete and smoother in thicker samples as in Figs. 1(d1)–1(d3). On the other hand, NM I can be associated with a typical field strength $\mathcal{B}_0 = \hbar/el_0^2$ with $l_0 = 2t/t_1$. Shown in Figs. 1(c1)–1(c3), although a mesoscopic thickness well hosts both NM I and II, NM I in thick samples may become less outstanding for small fields $|B| \ll \mathcal{B}_0$. In such a case, the monotonic contribution is densely accumulated through continuous momentum slices, which may outrun the contingent nontrivial occupation changes in Fig. 1(c0). However, as per Eq. (5), higher $|\mu|$ usually recovers and enhances nonmonotonicity by involving more bending LLs, e.g., in Fig. 1(c3). Therefore, while NM II remains exceptionally stable, a higher field or $|\mu|$ is beneficial to enhancing NM I in thicker samples.

Implications on experiments—Following such discussion, the magnetic field observation window for significant NM I is estimated to be approximately 10–60 T with the typical $\mathcal{B}_0 \sim 30$ T [21,41,42] (SM VI A). This is reachable with laboratory magnets and especially pulsed magnetic fields, which routinely go beyond 50 T and is widely used in magnetotransport [35,43–45]. On the other hand, NM II persists all along and will dominate more for μ closer to WPs. Besides, the nonmonotonic Hall effect is limited by $|B| \gtrsim |B|_c \sim \hbar^2 m_0/e\tau t_1^2$. When $\omega_c\tau < 1$ and relaxation becomes important, eventually the OHE prevails over quantum effects. Together with the realistic nondivergence that $G_H(B \to 0)$ approaches the AHE, they crucially regularize and suppress the apparently divergent downturn at small fields in Figs. 1(c) and 1(d) (SM III). This naturally benefits the nonmonotonic effect to reach smaller fields beyond the present calculation, which mainly accounts for the $\omega_c\tau > 1$ clean case.

Given that μ can vary in different materials or due to chemical doping, one might also observe the nonmonotonic $b < 0$, $\mu < 0$ case complementary to Figs. 1(c) and 1(d). In typical magnetic WSMs, the intrinsic magnetization withstands an antiparallel magnetic field up to a coercive field H_c about 0.1–10 T [9,28,34,46–48]. If the onset field of the LL is larger, one cannot enter deep into the nominal $b < 0$ regime for our system exhibiting magnetization in $\hat{z}$. However, once the magnetization is reversed by negative B, the inequalities (5) and (7) will also be reversed and nonmonotonicity is identically allowed (SM IV A). This relaxes the constraint of B, μ in experiments.

As aforementioned, various recent Hall measurements in magnetic WSMs show anomalously nonmonotonic (sometimes termed "nonlinear") field dependence, beyond the

OHE and AHE. They are typically observed in the regime $\omega_c\tau$ larger than or close to unity, where quantum effects appear and the major contribution is not found from extrinsic scatterings [25,26,28,35]. There has been no clear and consistent understanding, except, e.g., phenomenological fittings with electron and hole carriers. Our prediction qualitatively matches them and enables a promising physical picture: GdPtBi [25,26] and $Co_3Sn_2S_2$ with magnetization reversal measurements [28,33,34] typically confirm one nonmonotonic turn similar to Fig. 1(d3) of NM II when $|B| < 10$–15 T; PrAlSi at pulsed fields higher than 15 T [35] exhibits more complex nonmonotonic variation as Fig. 1(c3) of NM I suggests, which corroborates our estimation; PrAlSi [35] and GdPtBi [25] suggest deviation from conventional SdHE. Experiments also confirm the nondivergence at small $|B|$ as we envisaged. SM VI B presents a more thorough comparison and analysis. Despite the resemblance between these experiments and the theory, one should still keep in mind other possible contributions, e.g., more complex variation of the AHE induced by magnetic field [49,50].

In those systems with more than one pair of WPs, we can essentially consider multiple copies of the present model. Similar nonmonotonic contributions from other pairs will add up together in Hall signals. Given field $\boldsymbol{B}$, it is those momentum slices perpendicular to $\boldsymbol{B}$ that contribute, as long as $\boldsymbol{B}$ is not orthogonal to the WP pair alignment. It is, however, intriguing to note that Eq. (7) can render some WP pairs ineffective. This happens, e.g., when we have two pairs with opposite chirality-χ arrangements, one is thus not functioning. In other words, by observing nonmonotonicity experimentally, this chirality selectiveness can also help determine the topological configuration of the WP pairs (SM VI C).

We lastly emphasize an advantage of the present phenomenon. Unlike many other transport features of a WSM that typically rely on μ pinned to WPs, fine-tuning of μ is unnecessary. This strongly relaxes constraints on material choice and experimental setting. This remarkable property traces back to the following: the phenomenon utilizes the global topology in the WSM momentum space rather than any local feature close to WPs. For instance, with a thin film, WPs may often be gapped by the quantum confinement, against which the phenomenon remains robust.

Acknowledgments—We thank R. Yoshimi, I. Belopolski, M. Hirschberger, and Y. Xie for helpful discussions. This work was partially supported by the startup funding of Huazhong University of Science and Technology and JSPS KAKENHI (No. 24H00197 and No. 24H02231). N. N. was also supported by the RIKEN TRIP initiative. The computation was partially completed in the HPC Platform of Huazhong University of Science and Technology.

[1] G. E. Volovik, J. Phys. C **20**, L83 (1987).
[2] S. Murakami, New J. Phys. **9**, 356 (2007).
[3] X. Wan, A. M. Turner, A. Vishwanath, and S. Y. Savrasov, Phys. Rev. B **83**, 205101 (2011).
[4] B. Q. Lv, H. M. Weng, B. B. Fu, X. P. Wang, H. Miao, J. Ma, P. Richard, X. C. Huang, L. X. Zhao, G. F. Chen, Z. Fang, X. Dai, T. Qian, and H. Ding, Phys. Rev. X **5**, 031013 (2015).
[5] S.-Y. Xu *et al.*, Science **349**, 613 (2015).
[6] B. Yan and C. Felser, Annu. Rev. Condens. Matter Phys. **8**, 337 (2017).
[7] A. Burkov, Annu. Rev. Condens. Matter Phys. **9**, 359 (2018).
[8] N. P. Armitage, E. J. Mele, and A. Vishwanath, Rev. Mod. Phys. **90**, 015001 (2018).
[9] N. Nagaosa, T. Morimoto, and Y. Tokura, Nat. Rev. Mater. **5**, 621 (2020).
[10] B. Q. Lv, T. Qian, and H. Ding, Rev. Mod. Phys. **93**, 025002 (2021).
[11] K.-Y. Yang, Y.-M. Lu, and Y. Ran, Phys. Rev. B **84**, 075129 (2011).
[12] A. A. Burkov and L. Balents, Phys. Rev. Lett. **107**, 127205 (2011).
[13] G. Xu, H. Weng, Z. Wang, X. Dai, and Z. Fang, Phys. Rev. Lett. **107**, 186806 (2011).
[14] D. Bulmash, C.-X. Liu, and X.-L. Qi, Phys. Rev. B **89**, 081106(R) (2014).
[15] Z. Wang, M. G. Vergniory, S. Kushwaha, M. Hirschberger, E. V. Chulkov, A. Ernst, N. P. Ong, R. J. Cava, and B. A. Bernevig, Phys. Rev. Lett. **117**, 236401 (2016).
[16] H. Yang, Y. Sun, Y. Zhang, W.-J. Shi, S. S. P. Parkin, and B. Yan, New J. Phys. **19**, 015008 (2017).
[17] Y. J. Jin, R. Wang, Z. J. Chen, J. Z. Zhao, Y. J. Zhao, and H. Xu, Phys. Rev. B **96**, 201102(R) (2017).
[18] S. Nie, G. Xu, F. B. Prinz, and S. cheng Zhang, Proc. Natl. Acad. Sci. U.S.A. **114**, 10596 (2017).
[19] Q. Xu, E. Liu, W. Shi, L. Muechler, J. Gayles, C. Felser, and Y. Sun, Phys. Rev. B **97**, 235416 (2018).
[20] S. Borisenko, D. Evtushinsky, Q. Gibson, A. Yaresko, K. Koepernik, T. Kim, M. Ali, J. van den Brink, M. Hoesch, A. Fedorov, E. Haubold, Y. Kushnirenko, I. Soldatov, R. Schäfer, and R. J. Cava, Nat. Commun. **10**, 3424 (2019).
[21] S. Nie, Y. Sun, F. B. Prinz, Z. Wang, H. Weng, Z. Fang, and X. Dai, Phys. Rev. Lett. **124**, 076403 (2020).
[22] S. Nakatsuji, N. Kiyohara, and T. Higo, Nature (London) **527**, 212 (2015).
[23] X. Li, J. Koo, Z. Zhu, K. Behnia, and B. Yan, Nat. Commun. **14**, 1642 (2023).
[24] M. Hirschberger, S. Kushwaha, Z. Wang, Q. Gibson, S. Liang, C. A. Belvin, B. A. Bernevig, R. J. Cava, and N. P. Ong, Nat. Mater. **15**, 1161 (2016).
[25] T. Suzuki, R. Chisnell, A. Devarakonda, Y.-T. Liu, W. Feng, D. Xiao, J. W. Lynn, and J. G. Checkelsky, Nat. Phys. **12**, 1119 (2016).
[26] C. Shekhar *et al.*, Proc. Natl. Acad. Sci. U.S.A. **115**, 9140 (2018).
[27] S. Liang, J. Lin, S. Kushwaha, J. Xing, N. Ni, R. J. Cava, and N. P. Ong, Phys. Rev. X **8**, 031002 (2018).
[28] E. Liu *et al.*, Nat. Phys. **14**, 1125 (2018).

[29] Q. Wang, Y. Xu, R. Lou, Z. Liu, M. Li, Y. Huang, D. Shen, H. Weng, S. Wang, and H. Lei, Nat. Commun. **9**, 3681 (2018).

[30] D. F. Liu, A. J. Liang, E. K. Liu, Q. N. Xu, Y. W. Li, C. Chen, D. Pei, W. J. Shi, S. K. Mo, P. Dudin, T. Kim, C. Cacho, G. Li, Y. Sun, L. X. Yang, Z. K. Liu, S. S. P. Parkin, C. Felser, and Y. L. Chen, Science **365**, 1282 (2019).

[31] N. Morali, R. Batabyal, P. K. Nag, E. Liu, Q. Xu, Y. Sun, B. Yan, C. Felser, N. Avraham, and H. Beidenkopf, Science **365**, 1286 (2019).

[32] B. Jiang, L. Wang, R. Bi, J. Fan, J. Zhao, D. Yu, Z. Li, and X. Wu, Phys. Rev. Lett. **126**, 236601 (2021).

[33] S.-Y. Yang, J. Noky, J. Gayles, F. K. Dejene, Y. Sun, M. Dörr, Y. Skourski, C. Felser, M. N. Ali, E. Liu, and S. S. P. Parkin, Nano Lett. **20**, 7860 (2020).

[34] S. Li, G. Gu, E. Liu, P. Cheng, B. Feng, Y. Li, L. Chen, and K. Wu, ACS Appl. Electron. Mater. **2**, 126 (2020).

[35] L. Wu, S. Chi, H. Zuo, G. Xu, L. Zhao, Y. Luo, and Z. Zhu, npj Quantum Mater. **8**, 4 (2023).

[36] See Supplemental Material at http://link.aps.org/supplemental/10.1103/PhysRevLett.133.166301 for more details on models, analysis and calculations.

[37] A. J. Niemi and G. W. Semenoff, Phys. Rev. Lett. **51**, 2077 (1983); A. N. Redlich, Phys. Rev. Lett. **52**, 18 (1984).

[38] M. Mogi, Y. Okamura, M. Kawamura, R. Yoshimi, K. Yasuda, A. Tsukazaki, K. S. Takahashi, T. Morimoto, N. Nagaosa, M. Kawasaki, Y. Takahashi, and Y. Tokura, Nat. Phys. **18**, 390 (2022).

[39] H.-Z. Lu, W.-Y. Shan, W. Yao, Q. Niu, and S.-Q. Shen, Phys. Rev. B **81**, 115407 (2010).

[40] A. H. Castro Neto, F. Guinea, N. M. R. Peres, K. S. Novoselov, and A. K. Geim, Rev. Mod. Phys. **81**, 109 (2009).

[41] L. Muechler, E. Liu, J. Gayles, Q. Xu, C. Felser, and Y. Sun, Phys. Rev. B **101**, 115106 (2020).

[42] Z. Wang, Y. Sun, X.-Q. Chen, C. Franchini, G. Xu, H. Weng, X. Dai, and Z. Fang, Phys. Rev. B **85**, 195320 (2012).

[43] B. Fauqué, D. LeBoeuf, B. Vignolle, M. Nardone, C. Proust, and K. Behnia, Phys. Rev. Lett. **110**, 266601 (2013).

[44] M. Uchida, S. Sato, H. Ishizuka, R. Kurihara, T. Nakajima, Y. Nakazawa, M. Ohno, M. Kriener, A. Miyake, K. Ohishi, T. Morikawa, M. S. Bahramy, T. hisa Arima, M. Tokunaga, N. Nagaosa, and M. Kawasaki, Sci. Adv. **7**, eabl5381 (2021).

[45] M. Kondo, M. Ochi, R. Kurihara, A. Miyake, Y. Yamasaki, M. Tokunaga, H. Nakao, K. Kuroki, T. Kida, M. Hagiwara, H. Murakawa, N. Hanasaki, and H. Sakai, Phys. Rev. B **107**, L121112 (2023).

[46] G. S. Thakur, P. Vir, S. N. Guin, C. Shekhar, R. Weihrich, Y. Sun, N. Kumar, and C. Felser, Chem. Mater. **32**, 1612 (2020).

[47] J. Ikeda, K. Fujiwara, J. Shiogai, T. Seki, K. Nomura, K. Takanashi, and A. Tsukazaki, Commun. Mater. **2**, 18 (2021).

[48] N. Yoshikawa, K. Ogawa, Y. Hirai, K. Fujiwara, J. Ikeda, A. Tsukazaki, and R. Shimano, Commun. Phys. **5**, 328 (2022).

[49] N. Nagaosa, J. Sinova, S. Onoda, A. H. MacDonald, and N. P. Ong, Rev. Mod. Phys. **82**, 1539 (2010).

[50] K. S. Takahashi, H. Ishizuka, T. Murata, Q. Y. Wang, Y. Tokura, N. Nagaosa, and M. Kawasaki, Sci. Adv. **4**, eaar7880 (2018).